

This is the accepted manuscript made available via CHORUS. The article has been published as:

Density response of a trapped Fermi gas: A crossover from the pair vibration mode to the Goldstone mode

A. Korolyuk, J. J. Kinnunen, and P. Törmä

Phys. Rev. A **84**, 033623 — Published 19 September 2011

DOI: [10.1103/PhysRevA.84.033623](https://doi.org/10.1103/PhysRevA.84.033623)

Density response of a trapped Fermi gas: a crossover from the pair vibration mode to the Goldstone mode

A. Korolyuk¹, J. J. Kinnunen¹, P. Törmä^{1,2*}

¹*Department of Applied Physics, School of Science,
Aalto University, P.O. Box 15100, 00076 Aalto, Finland*

²*Kavli Institute for Theoretical Physics, University of California, Santa Barbara, California 93106-4030, USA*

We consider the density response of a trapped two-component Fermi gas. Combining the Bogoliubov-deGennes method with the random phase approximation allows the study of both collective and single particle excitations. Calculating the density response across a wide range of interactions, we observe a crossover from a weakly interacting pair vibration mode to a strongly interacting Goldstone mode. The crossover is associated with a depressed collective mode frequency and an increased damping rate, in agreement with density response experiments performed in strongly interacting atomic gases.

I. INTRODUCTION

The response of a many-body system to external perturbations can be understood in terms of collective, i.e. many-body, and single particle excitations. Collective modes of a quantum fluid are well described by the hydrodynamic model in the strongly interacting hydrodynamic and the weakly interacting collisionless limits [1–5]. However, experimental studies on collective modes of trapped Fermi gases [6–9] yielded surprises [10–12] that did not fit in the simple picture obtained from the hydrodynamic theory. The difference was suggested to lie in the interplay between the single particle excitations and the collective modes [13].

The Bogoliubov-deGennes (BdG) mean-field theory provides a microscopic description of the trapped Fermi gas. While the single particle excitations are readily accessible from the basic BdG theory, also the collective modes can be obtained by using the random phase approximation [14] (RPA). The method allows the study of different modes [15–18], but here we will concentrate on the monopole mode in a spherically symmetric trapped Fermi gas. The method has already been used for studying the monopole mode of a trapped Fermi gas in the limits of weak and strong interactions. The purpose of the present work is to study the interesting crossover region between the weakly interacting and the strongly interacting regimes where the hydrodynamic theory has failed to properly describe the experiments.

The weakly interacting limit was studied in Ref. [19], and in this limit the lowest lying collective mode with the monopole symmetry was identified as the pair vibration mode with the frequency $\omega = 2\Delta(0)/\hbar$, where $\Delta(0)$ is the superfluid excitation gap in the center of the trap. This mode was argued to be the precursor of the Goldstone mode in the strongly interacting regime with the frequency $2\omega_T$, where ω_T is the harmonic trapping frequency, in agreement with the strongly interacting hy-

drodynamic theory. The Goldstone mode in this more strongly interacting regime was considered in Ref. [20].

Here we study the actual transition between the two regimes and how the collective pair vibration mode transforms into the collective Goldstone mode when the interaction strength is increased. The crossover region is characterized by a depression of the collective mode frequencies and increased damping, in qualitative agreement with experiments done in non-spherically symmetric traps and with various collective modes [10–12]. The full crossover could be studied in future experiments, and the study of the lately realized systems with small numbers of atoms [21] might be helpful in finding the required parameters.

This paper is organised as follows. In Section II we review the standard theory of linear response for a small disturbance to the system and discuss the connection between the density response and the frequency of collective excitations. In Section III we discuss the details of the methods used. In Section IV we present and analyse our results and Section V summarises the main findings and conclusions of this work.

II. LINEAR RESPONSE AND COLLECTIVE BEHAVIOUR

In this section we review the calculation showing the connection between the density response and the frequency of collective excitations of a system. This shows how peaks in the imaginary part of the density response function correspond to the frequencies of collective excitations, providing the theoretical background for interpreting the results of the numerically calculated density response function.

A. The density response function

Let us consider a system described by a full many-body Hamiltonian \hat{H} . It is assumed that the system is initially in a pure state $|\phi_0\rangle$ which is an eigenstate of

* paivi.torma@aalto.fi

the Hamiltonian \hat{H} , for example the ground state. At the moment $t = 0$ a probing field or a perturbation \hat{V} is switched on. From that moment the system evolves under the Hamiltonian $\hat{H}' = \hat{H} + \hat{V}$. We denote the state of the system at the time t as $|\phi(t)\rangle$. In the absence of any probing field, the state of the system at time t would remain $|\phi_0\rangle$. The difference between $|\phi(t)\rangle$ and $|\phi_0\rangle$ is thus caused by the probing field \hat{V} . This difference can be measured with the help of an observable $\hat{O}(\mathbf{r})$. Without the probing field, the average of the operator $\hat{O}(\mathbf{r})$ (the statistical average after a series of measurements) would be

$$O_0(\mathbf{r}) = \langle \phi_0 | \hat{O}(\mathbf{r}) | \phi_0 \rangle. \quad (1)$$

When the field \hat{V} is switched on, the measurements would yield

$$O(\mathbf{r}, t) = \langle \phi(t) | \hat{O}(\mathbf{r}) | \phi(t) \rangle. \quad (2)$$

The difference

$$\delta O(\mathbf{r}, t) = O(\mathbf{r}, t) - O_0(\mathbf{r}) \quad (3)$$

indicates how the perturbation \hat{V} has influenced the physical observable \hat{O} .

The difference, or response, δO can be calculated in the interaction picture representation. In the density response approach we consider \hat{V} as a weak disturbance to the system. In this case we can take into account only the first (linear) order of the perturbation \hat{V} . Thus the response is

$$\delta O(\mathbf{r}, t) \approx -i \int_{-\infty}^t dt' \langle \phi_0 | [\hat{O}_I(\mathbf{r}, t), \hat{V}_I(t')] | \phi_0 \rangle, \quad (4)$$

where \hat{O}_I and \hat{V}_I are the operators \hat{O} and \hat{V} in the interaction picture representation.

In this work we are interested in the particular case of an external potential $v(\mathbf{r}, t)$ that couples to the density $\hat{\rho}(\mathbf{r})$, corresponding to an operator $\hat{V} = \int d\mathbf{r} \hat{\rho}(\mathbf{r}) v(\mathbf{r}, t)$. Then δO becomes

$$\delta O(\mathbf{r}, t) = \int_{-\infty}^{+\infty} dt' d\mathbf{r}' \mathcal{A}(\mathbf{r}, \mathbf{r}', t, t') v(\mathbf{r}', t'), \quad (5)$$

where the kernel

$$\mathcal{A}(\mathbf{r}, \mathbf{r}', t, t') = -i \langle \phi_0 | [\hat{O}_I(\mathbf{r}, t), \hat{\rho}_I(\mathbf{r}', t')] | \phi_0 \rangle \theta(t - t') \quad (6)$$

is called the response function.

The response function $\mathcal{A}(\mathbf{r}, \mathbf{r}', t, t')$ in Eq. (6) shows the change in the observable \hat{O} measured at the point (\mathbf{r}, t) due to the infinitesimally small perturbation at the point (\mathbf{r}', t') . If the Hamiltonian \hat{H} does not depend on time, then the time-dependence of \mathcal{A} will be on the difference $t - t'$ only.

The derivation above holds for any general observable \hat{O} . In the special case $\hat{O} = \hat{\rho}$, i.e. when the observed quantity is also the density, the response function is called the density response function, and the expression for it is

$$\mathcal{A}(\mathbf{r}, \mathbf{r}', t - t') = -i \langle \phi_0 | [\hat{\rho}_I(\mathbf{r}, t), \hat{\rho}_I(\mathbf{r}', t')] | \phi_0 \rangle \theta(t - t'). \quad (7)$$

B. The frequency of the collective excitations in the density response

After a Fourier transformation of Eq. (7) one obtains

$$\mathcal{A}(\mathbf{r}, \mathbf{r}', \omega) = -i \int_{-\infty}^0 dt e^{-i\omega t} \langle \phi_0 | [\hat{\rho}_I(\mathbf{r}, 0), \hat{\rho}_I(\mathbf{r}', t)] | \phi_0 \rangle. \quad (8)$$

We assume, formally, that the Hamiltonian \hat{H} is diagonalized, and E_n and $|n\rangle$ are its eigenvalues and eigenvectors: $\hat{H} |n\rangle = E_n |n\rangle$, $n = 0, 1, \dots$. As eigenstates of a hermitian operator, the eigenvectors are orthogonal $\langle n | n' \rangle = \delta_{n, n'}$ and form a complete basis $\sum_n |n\rangle \langle n| = \hat{1}$. One can assume that the initial state of the system, earlier denoted as $|\phi_0\rangle$, is the ground state $|0\rangle$: $|\phi_0\rangle \equiv |0\rangle$.

Transforming back to the Schrödinger picture representation $\hat{\rho}_I(\mathbf{r}, t) = e^{i\hat{H}t} \hat{\rho} e^{-i\hat{H}t}$, Eq. (8) becomes

$$\mathcal{A}(\mathbf{r}, \mathbf{r}', \omega) = 2 \int_{-\infty}^0 dt e^{-i\omega t} \text{Im} (e^{-iE_0 t} \langle \phi_0 | \hat{\rho}(\mathbf{r}) e^{i\hat{H}t} \hat{\rho}(\mathbf{r}') | \phi_0 \rangle) \quad (9)$$

Using the completeness of the eigenbasis and performing the time integral yields

$$\mathcal{A}(\mathbf{r}, \mathbf{r}', \omega) = \sum_n \frac{\langle \phi_0 | \hat{\rho}(\mathbf{r}) | n \rangle \langle n | \hat{\rho}(\mathbf{r}') | \phi_0 \rangle}{\omega - (E_n - E_0)} - \frac{\langle \phi_0 | \hat{\rho}(\mathbf{r}') | n \rangle \langle n | \hat{\rho}(\mathbf{r}) | \phi_0 \rangle}{\omega + (E_n - E_0)}. \quad (10)$$

Thus, the density response $\mathcal{A}(\mathbf{r}, \mathbf{r}', \omega)$ yields information about the excitation spectrum of the system $E_n - E_0$. In Section IV we will analyse the numerically calculated density response function and identify the poles of Eq. (10), i.e. the frequencies ω in which \mathcal{A} has peaks, as the collective or single particle excitation frequencies. Note that here, formally, E_n includes all excitations of the system, both collective and single particle ones.

III. THE RANDOM PHASE APPROXIMATION FOR THE HARMONIC TRAP GEOMETRY

In the previous section we discussed the general definitions of density response function and its connection to

the collective excitation frequencies. Here we will apply the random phase approximation (RPA) [14, 22] to express the density response using Green's functions. These in turn will be solved using the Bogoliubov-deGennes (BdG) mean-field theory, allowing an efficient solution of the density response for a spherically symmetric trapped atomic gas.

A. Density response expressed using Green's functions

A dilute ultracold two-component atomic gas trapped in a spherically symmetric trap can be described with the Hamiltonian

$$\hat{H} = \hat{K} + \hat{U}, \quad (11)$$

where

$$\hat{K} = \sum_{\alpha=\{\uparrow,\downarrow\}} \int d\mathbf{r} \psi_{\alpha}^{\dagger}(\mathbf{r}) \left[\frac{-\nabla^2}{2m} - \mu + \frac{m\omega_T r^2}{2} \right] \psi_{\alpha}(\mathbf{r}) \quad (12)$$

is the single particle Hamiltonian containing the kinetic energy and the harmonic trapping potential of frequency ω_T , $\psi_{\alpha}^{(\dagger)}(\mathbf{r})$ is the annihilation (creation) operator of an atom in a state α at point \mathbf{r} , and

$$\hat{U} = \frac{1}{2} \sum_{\alpha,\beta=\{\uparrow,\downarrow\}} \int d\mathbf{r} d\mathbf{r}' \psi_{\alpha}^{\dagger}(\mathbf{r}') \psi_{\beta}^{\dagger}(\mathbf{r}') \psi_{\beta}(\mathbf{r}) \psi_{\alpha}(\mathbf{r}) g(\mathbf{r}' - \mathbf{r}) \quad (13)$$

describes two-body interactions. The short-range interactions can be described by the two-body scattering T-matrix in the contact potential approximation $g(\mathbf{r}' - \mathbf{r}) = g_0 \delta(\mathbf{r}' - \mathbf{r})$, where the coupling constant g_0 is related to the physical s-wave scattering length through the relation $1/g_0 = \frac{m}{4\pi a} - \sum_k \frac{1}{2\epsilon_k}$ [23]. Eq. (13) becomes

$$\hat{U} = \frac{g_0}{2} \sum_{\alpha,\beta=\{\uparrow,\downarrow\}} \int d\mathbf{r} \psi_{\alpha}^{\dagger}(\mathbf{r}) \psi_{\beta}^{\dagger}(\mathbf{r}) \psi_{\beta}(\mathbf{r}) \psi_{\alpha}(\mathbf{r}). \quad (14)$$

For the calculation of the density response we need to add a weak probing field \hat{V} (for more details see II A). We consider

$$\hat{V} = \int d\mathbf{r} [\phi_{\uparrow}(\mathbf{r}, t) n_{\uparrow}(\mathbf{r}) + \phi_{\downarrow}(\mathbf{r}, t) n_{\downarrow}(\mathbf{r}) + \eta(\mathbf{r}, t) \psi_{\downarrow}(\mathbf{r}) \psi_{\uparrow}(\mathbf{r}) + H.c.]. \quad (15)$$

The three terms in \hat{V} allow the calculation of the density responses to the three external fields $\phi_{\uparrow}(\mathbf{r}, t)$, $\phi_{\downarrow}(\mathbf{r}, t)$, $\eta(\mathbf{r}, t)$, which couple to the system in different ways. To simplify the notation, we consider a response to a generic field $h(\mathbf{r}, t)$, where $h(\mathbf{r}, t)$ can be any of these three external fields.

As physical observables for which we will analyse the response, we consider the densities ρ_{\uparrow} and ρ_{\downarrow} of up and

down components, respectively. Additionally, we consider the response of the order parameter $\Delta(\mathbf{r})$ to the probing field. We expect that the same frequencies of collective excitations will appear in all three responses; naturally, this can be confirmed numerically.

A useful way of formulating the density response is by using the two-point Green's functions $G_{ij}(\mathbf{1}, \mathbf{2}) = -\langle T \Psi_i(\mathbf{1}) \Psi_j^{\dagger}(\mathbf{2}) \rangle$ in the Nambu formalism, where $\mathbf{1}$ denotes space-time point \mathbf{x}_1, t_1 and $\Psi(\mathbf{1}) = \begin{bmatrix} \psi_{\uparrow}(\mathbf{1}) \\ \psi_{\downarrow}^{\dagger}(\mathbf{1}) \end{bmatrix}$. The Green's function for $\mathbf{1} = \mathbf{2}$ has a simple physical meaning:

$$\hat{G}(\mathbf{1}, \mathbf{1}) = \begin{pmatrix} \rho_{\uparrow}(\mathbf{1}) & \Delta(\mathbf{1}) \\ \Delta^*(\mathbf{1}) & -\rho_{\downarrow}(\mathbf{1}) \end{pmatrix}, \quad (16)$$

where $\rho_{\uparrow}(\mathbf{1}), \rho_{\downarrow}(\mathbf{1})$ are the densities and $\Delta(\mathbf{1})$ is the order parameter, i.e. the gap at the point $\mathbf{1} = (\mathbf{x}_1, t_1)$.

We consider the response of the Green's function:

$$\delta \hat{G}_{ij}(\mathbf{1}, \mathbf{2}) = \int_{-\infty}^{+\infty} dt_5 \int_V d\mathbf{x}_5 A_{ij}(\mathbf{1}, \mathbf{2}, \mathbf{5}) h(\mathbf{5}). \quad (17)$$

This can be interpreted as the change of the Green's function, or how the transition between the points (\mathbf{x}_1, t_1) and (\mathbf{x}_2, t_2) alters due to a probing field h at the point (\mathbf{x}_5, t_5) . The kernel can be written as

$$A_{ij}(\mathbf{1}, \mathbf{2}, \mathbf{5}) = \left. \frac{\delta G_{ij}(\mathbf{1}, \mathbf{2})}{\delta h(\mathbf{5})} \right|_{h \rightarrow 0}. \quad (18)$$

For the one-point Green's functions the response is

$$\delta \hat{G}_{ij}(\mathbf{1}, \mathbf{1}) = \int_{-\infty}^{+\infty} dt_5 \int_V d\mathbf{x}_5 \tilde{A}_{ij}(\mathbf{1}, \mathbf{5}) h(\mathbf{5}), \quad (19)$$

where

$$\tilde{A}_{ij}(\mathbf{1}, \mathbf{3}) \equiv A_{ij}(\mathbf{1}, \mathbf{1}, \mathbf{3}) \quad (20)$$

and

$$\tilde{A}_{ij}(\mathbf{1}, \mathbf{5}) = \left. \frac{\delta G_{ij}(\mathbf{1}, \mathbf{1})}{\delta h(\mathbf{5})} \right|_{h \rightarrow 0}. \quad (21)$$

As in Eq. (16), this is a 2x2 matrix with the different elements describing the response to different fields. For example, the response of the density of up particles $\tilde{A}_{\uparrow\uparrow}(\mathbf{1}, \mathbf{5})$ is

$$\delta \rho_{\uparrow}(\mathbf{1}) = \int_{-\infty}^{+\infty} dt_5 \int_V d\mathbf{x}_5 \tilde{A}_{\uparrow\uparrow}(\mathbf{1}, \mathbf{5}) h(\mathbf{5}). \quad (22)$$

Starting from the Hamiltonian (11) and using the random-phase approximation (RPA) [22], we write (for more details see Appendix A)

$$A_{ij}(\mathbf{1}, \mathbf{2}, \mathbf{5}) = A_{0ij}(\mathbf{1}, \mathbf{2}, \mathbf{5}) + g_0 \sum_{k,l} \int d\mathbf{3} L_{ikkj}(\mathbf{1}, \mathbf{2}, \mathbf{3}) A_{ll}(\mathbf{3}, \mathbf{3}, \mathbf{5}) - g_0 \sum_{k,l} \int d\mathbf{3} L_{iklj}(\mathbf{1}, \mathbf{2}, \mathbf{3}) A_{kl}(\mathbf{3}, \mathbf{3}, \mathbf{5}), \quad (23)$$

where $L_{iklj}(\mathbf{1}, \mathbf{2}, \mathbf{3}) = G_{ik}(\mathbf{1}, \mathbf{3}) G_{lj}(\mathbf{3}, \mathbf{2})$, and $A_0(\mathbf{1}, \mathbf{2}, \mathbf{5}) = L_{i\uparrow\uparrow j}(\mathbf{1}, \mathbf{2}, \mathbf{5})$, $L_{i\downarrow\downarrow j}(\mathbf{1}, \mathbf{2}, \mathbf{5})$, $L_{i\uparrow\downarrow j}(\mathbf{1}, \mathbf{2}, \mathbf{5}) + L_{i\downarrow\uparrow j}(\mathbf{1}, \mathbf{2}, \mathbf{5})$ for $h = \phi_\uparrow, \phi_\downarrow, \eta$ respectively. For the density response $\tilde{A}_{ij}(\mathbf{1}, \mathbf{5})$ the equation in Eq. (23) becomes

$$\tilde{A}_{ij}(\mathbf{1}, \mathbf{5}) = \tilde{A}_{0ij}(\mathbf{1}, \mathbf{5}) + g_0 \sum_{k,l} \int d\mathbf{3} \tilde{L}_{ikkj}(\mathbf{1}, \mathbf{3}) \tilde{A}_{ll}(\mathbf{3}, \mathbf{5}) - g_0 \sum_{k,l} \int d\mathbf{3} \tilde{L}_{iklj}(\mathbf{1}, \mathbf{3}) \tilde{A}_{kl}(\mathbf{3}, \mathbf{5}), \quad (24)$$

where $\tilde{L}_{iklj}(\mathbf{1}, \mathbf{3}) = G_{ik}(\mathbf{1}, \mathbf{3}) \tilde{G}_{lj}(\mathbf{3}, \mathbf{1})$ and $\tilde{A}_{0ij}(\mathbf{1}, \mathbf{5})$ is correspondingly expressed via $\tilde{L}_{iklj}(\mathbf{1}, \mathbf{3})$.

B. Spherical symmetry and the angular momentum

Solving even the mean-field density response in Eq. (24) in a spatially inhomogeneous system such as the trapped gas is a numerically very demanding task. However, taking advantage of the assumed spherical symmetry of the system, the Eq. (24) can be greatly simplified by expressing all quantities in spherical coordinates. The spherical symmetry implies separation of different angular momentum responses, allowing a significant simplification of the numerical calculations.

Expressing the response function using Legendre polynomials (and using the knowledge that the response function depends only on the time difference $t_1 - t_2$) yields

$$\tilde{A}_{ik}(\mathbf{1}, \mathbf{2}) = \sum_{L,\omega} \mathcal{A}_{ik,L}(r_1, r_2, \omega) P_L(\cos \gamma) e^{-i\omega(t_1 - t_2)}, \quad (25)$$

where ω is a frequency (can be either real or imaginary), $P_L(\cos \gamma)$ is the Legendre polynomial, and γ is the angle between the vectors \mathbf{r}_1 and \mathbf{r}_2 . Other functions involved in the solution, such as the Green's function $\tilde{G}_{ik}(\mathbf{1}, \mathbf{3})$ and $L_{iklj}(\mathbf{1}, \mathbf{2}, \mathbf{3})$ can be decomposed in the same way. Instead of eight parameters $\mathbf{r}_1, t_1, \mathbf{r}_2, t_2$ all the functions now depend only on four parameters: r_1, r_2 (magnitudes of the vectors \mathbf{r}_1 and \mathbf{r}_2), ω (frequency) and L (angular momentum).

With this decomposition, Eq. (23) simplifies to

$$\begin{aligned} \mathcal{A}_{ij,L}(r_1, r_5, \omega) &= \mathcal{A}_{0ij,L}(r_1, r_5, \omega) \\ &+ g_0 \frac{4\pi}{2L+1} \int r_3^2 dr_3 \mathcal{L}_{ikkj,L}(r_1, r_3, \omega) \mathcal{A}_{ll,L}(r_3, r_5, \omega) \\ &- g_0 \frac{4\pi}{2L+1} \int r_3^2 dr_3 \mathcal{L}_{iklj,L}(r_1, r_3, \omega) \mathcal{A}_{kl,L}(r_3, r_5, \omega). \end{aligned} \quad (26)$$

As explained in Section II B, the peaks in the density response $\mathcal{A}_{ij,L}(r_1, r_5, \omega)$ yield the frequencies of collective excitations, now corresponding to a specific angular momentum L . For example, in this work we will study the case $L = 0$, in other words the spherically symmetric monopole mode collective excitation.

In the Section III C we calculate the coefficient $\mathcal{L}_{ikkj,L}(r_1, r_3, \omega)$ via the Bogoliubov-deGennes approximation. In Section III D we consider the simplifications we need to proceed from the analytical equations to the numerical calculations.

C. Green's functions in the Bogoliubov-deGennes approach

In this section we will use the mean-field Bogoliubov-deGennes (BdG) method to obtain the single particle Green's functions in the trap, thus allowing the numerical solution of the density response. The Bogoliubov-deGennes equations can be obtained by approximating the interaction part of the Hamiltonian (13) by a quadratic form

$$U = - \int d\mathbf{r} \psi_\uparrow^\dagger(\mathbf{r}) \psi_\downarrow^\dagger(\mathbf{r}) \Delta(\mathbf{r}) + H.c., \quad (27)$$

where $\Delta(\mathbf{r}) = |g_0| \langle \psi_\uparrow(\mathbf{r}) \psi_\downarrow(\mathbf{r}) \rangle$ is the order parameter. The Hartree energy is $g_0 \int d\mathbf{r} \left(\psi_\uparrow^\dagger(\mathbf{r}) \psi_\uparrow(\mathbf{r}) n_\downarrow(\mathbf{r}) + \psi_\downarrow^\dagger(\mathbf{r}) \psi_\downarrow(\mathbf{r}) n_\uparrow(\mathbf{r}) \right)$, where $n_{\uparrow(\downarrow)}(\mathbf{r})$ is the density of up(down) particles. Most of the results below neglect the Hartree energy because, especially for strong interactions $|k_F a| \sim 1$, the inclusion of the Hartree energy would require a prohibitively high cutoff energy, which is a critical quantity for the efficiency of the numerical method. However, we will briefly consider below the effect of the Hartree energy shift in the weakly interacting regime.

The present work is concentrated in the moderate to weak interaction regime $|k_F a| \lesssim 1$, and the effect of the Hartree energy is to compress the gas slightly, increasing the order parameter at the centre of the trap [24]. As will be seen in Section IV, the key quantity for the density response is the order parameter profile instead of the interaction strength. Consequently the results will be shown as a function of the order parameter at the centre of the trap $\Delta(r=0)$. The compressing effect of the Hartree energy is thus relevant for finding the precise correspondence between the system input parameters (atom numbers, masses, trap frequencies, temperature, and interaction strength) and the order parameter. However, as will be seen, the Hartree energy does not change the qualitative features of the density response.

With these approximations the Hamiltonian in Eq. (11) becomes quadratic in $\psi_\alpha(\mathbf{r})$:

$$H = \sum_{\alpha=\{\uparrow,\downarrow\}} \int d\mathbf{r} \psi_\alpha^\dagger(\mathbf{r}) \left[-\frac{\hbar^2 \nabla^2}{2m} - \mu + \frac{m\omega_T^2 r^2}{2} \right] \psi_\alpha(\mathbf{r}) + \int d\mathbf{r} \psi_\uparrow^\dagger(\mathbf{r}) \psi_\downarrow^\dagger(\mathbf{r}) \Delta(\mathbf{r}) + H.c. \quad (28)$$

The fermion fields can be expressed in the harmonic oscillator basis as $\psi_\alpha(\mathbf{r}) = \sum_{nlm} R_{nl}(r) Y_{lm}(\theta) c_{nlm\alpha}$, where the operator $c_{nlm\sigma}$ destroys an atom from the harmonic oscillator eigenstate nlm , $Y_{lm}(\theta)$ are the spherical harmonics, and the radial eigenstates are given by

$$R_{nl}(r) = \sqrt{2}(m\omega_T)^{3/4} \sqrt{\frac{n!}{(n+l+1/2)!}} e^{-\bar{r}^2/2} \bar{r}^l L_n^{l+1/2}(\bar{r}^2), \quad (29)$$

where $L_n^{l+1/2}(\bar{r}^2)$ is the associated Laguerre polynomial and $\bar{r} \equiv r \sqrt{\frac{m\omega_T}{\hbar}}$.

The Hamiltonian in Eq. (28) can be diagonalized using a canonical transformation

$$c_{nlm\uparrow} = \sum_{j=1}^N W_{n,j}^l \gamma_{jlm\uparrow} + (-1)^m \sum_{j=1}^N W_{n,N+j}^l \gamma_{jlm\downarrow}^\dagger \quad (30)$$

and

$$c_{nlm\downarrow}^\dagger = (-1)^m \sum_{j=1}^N W_{N+n,j}^l \gamma_{jlm\uparrow}^\dagger + \sum_{j=1}^N W_{N+n,N+j}^l \gamma_{jlm\downarrow}^\dagger \quad (31)$$

which yields the diagonalized Hamiltonian

$$H = \sum_{jlm,\alpha} E_{jl} \gamma_{jlm\alpha}^\dagger \gamma_{jlm\alpha}. \quad (32)$$

The index j in $\gamma_{jlm\alpha}$ corresponds to the enumeration of the quasiparticle states, the index l is the angular momentum, and $m = -l, -l+1, \dots, l$ is the z -component of the angular momentum. The index α does not have the meaning of a physical (pseudo)spin anymore, but it has an auxiliary function.

The equation for the order parameter profile at zero temperature is

$$\Delta(r) = g_0 \sum_{nn'lj} \frac{2l+1}{4\pi} R_{nl}(r) R_{n'l}(r) W_{n,j}^l W_{N+n',j}^l, \quad (33)$$

which needs to be solved self-consistently together with the number equations for the local atom densities

$$n_\uparrow(r) = \sum_{nn'lj} \frac{2l+1}{4\pi} R_{nl}(r) R_{n'l}(r) W_{n,j}^l W_{n',j}^l, \quad (34)$$

and

$$n_\downarrow(r) = \sum_{nn'lj} \frac{2l+1}{4\pi} R_{nl}(r) R_{n'l}(r) W_{N+n,j}^l W_{N+n',j}^l. \quad (35)$$

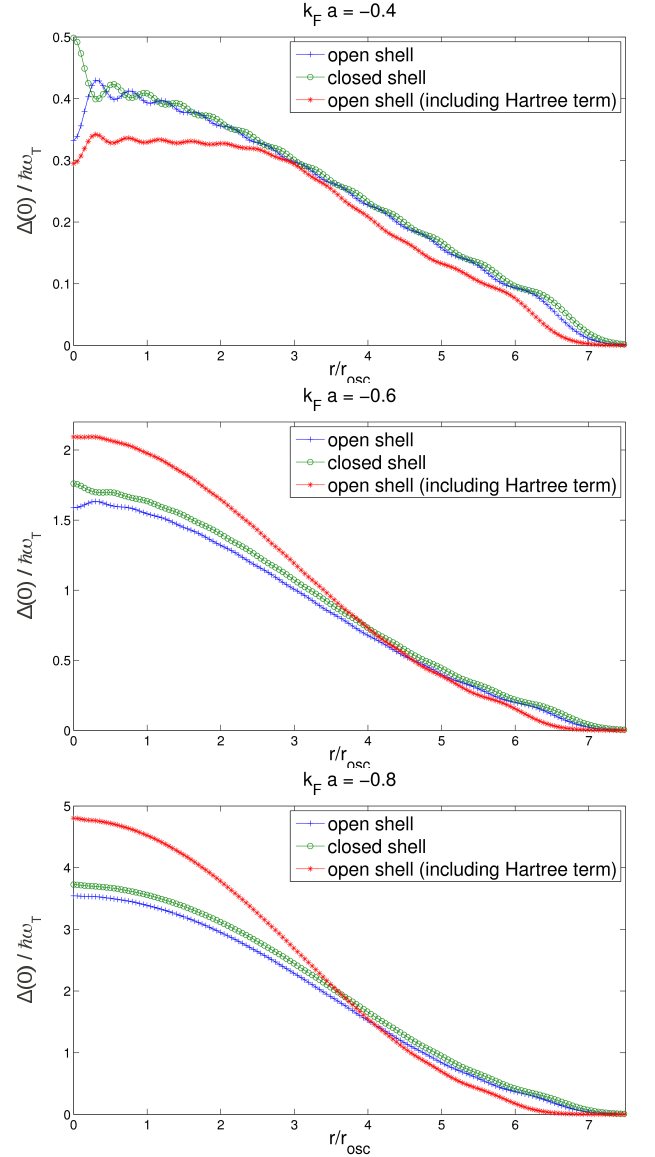


FIG. 1. (Color online) Order parameter profiles $\Delta(r)$ obtained using the Bogoliubov-deGennes method for different interaction strengths. Open and closed shell data correspond to different total atom numbers, $N = 4930$ and $N = 5600$, respectively. Shown are also the profiles that include the Hartree energy shift contribution, calculated for $N = 4930$. Figures show data for $k_F a = -0.4$, $k_F a = -0.6$ and $k_F a = -0.8$.

Fig. 1 shows the order parameter profiles $\Delta(r)$ for different atom numbers, interaction strengths, and also with the Hartree energy shift.

We calculate the coefficients $W_{n,j}^l$ and the eigenenergies E_{jl} numerically. The Green's function $G_{ij}(\mathbf{1}, \mathbf{2})$ can

be expressed via $W_{n,j}^l$:

$$\hat{G}(\mathbf{r}_1, \mathbf{r}_2, \Omega_n) = - \sum_l \frac{2l+1}{4\pi} P_l(\cos \theta_{12}) \times \left(\frac{\Lambda_{jl}^-(r_1) \Lambda_{jl}^{+\dagger}(r_2)}{i\Omega_n - E_{jl}} + \frac{\Lambda_{jl}^+(r_1) \Lambda_{jl}^{+\dagger}(r_2)}{i\Omega_n + E_{jl}} \right). \quad (36)$$

$$\begin{aligned} \mathcal{L}_{iklj,L}(r_1, r_3, \omega) = & (2L+1) \sum_{L_1 L_2} \begin{pmatrix} L & L_1 & L_2 \\ 0 & 0 & 0 \end{pmatrix}^2 \frac{2L_1+1}{4\pi} \frac{2L_2+1}{4\pi} \\ & * \sum_{J_1 J_2} \left(\lambda_{J_1 L_1, ik}^- \lambda_{J_2 L_2, lj}^- \frac{n_F(E_{J_1 L_1}) - n_F(E_{J_2 L_2})}{\omega + E_{J_1 L_1} - E_{J_2 L_2}} + \lambda_{J_1 L_1, ik}^+ \lambda_{J_2 L_2, lj}^+ \frac{n_F(-E_{J_1 L_1}) - n_F(-E_{J_2 L_2})}{\omega - E_{J_1 L_1} + E_{J_2 L_2}} \right. \\ & \left. + \lambda_{J_1 L_1, ik}^- \lambda_{J_2 L_2, lj}^+ \frac{n_F(E_{J_1 L_1}) - n_F(-E_{J_2 L_2})}{\omega + E_{J_1 L_1} + E_{J_2 L_2}} + \lambda_{J_1 L_1, ik}^+ \lambda_{J_2 L_2, lj}^- \frac{n_F(-E_{J_1 L_1}) - n_F(E_{J_2 L_2})}{\omega - E_{J_1 L_1} - E_{J_2 L_2}} \right). \end{aligned} \quad (37)$$

Here the occupation numbers are given by the Fermi-Dirac equation $n_F(E) = \frac{1}{\exp(\beta E) + 1}$ at the temperature $k_B T = \frac{1}{\beta}$. Furthermore, $\begin{pmatrix} L & L_1 & L_2 \\ 0 & 0 & 0 \end{pmatrix}$ are the Wigner 3j-symbols. Finally, $\lambda_{J_1 L_1, ik}^\pm = \Lambda_{J_1 L_1, i}^\pm(r_1) \Lambda_{J_1 L_1, k}^{\pm\dagger}(r_3)$ and $\lambda_{J_2 L_2, lj}^\pm = \Lambda_{J_2 L_2, l}^\pm(r_3) \Lambda_{J_2 L_2, j}^{\pm\dagger}(r_1)$.

In this section we have derived the kernel of the Eq. (26), $\mathcal{L}_{iklj,L}(r_1, r_3, \omega)$, as a function of the coefficients $W_{n,j}^l$ and the eigenenergies E_{jl} , which are to be calculated numerically. Thus Eq. (26) can be solved, and the resulting density response can be obtained.

D. Basic definitions for numerical calculations

In this section we will discuss the parameters used in the numerical calculations. As noted in Eq. (12), the gas of atoms of mass m is confined in the harmonic trapping potential of a frequency ω_T . The system is characterised by two units: the unit of energy (the difference between neighbouring levels) $\hbar\omega_T$ and the unit of length (the oscillator length) $r_{\text{osc}} = \sqrt{\frac{\hbar}{m\omega_T}}$. In the numerical calculations we use dimensionless values, in the unit system based on $\hbar\omega_T$ and r_{osc} .

The interaction strength is determined by the two-body scattering length a as $1/g_0 = \frac{m}{4\pi\hbar^2 a} - \gamma(r)$ where the position dependent renormalization coefficient is calculated in the local density approximation [25] and is

where $\Lambda_{jl}^-(r) = \sum_n \begin{pmatrix} W_{n,N+j}^l \\ W_{N+n,N+j}^l \end{pmatrix} R_{nl}(r)$, $\Lambda_{jl}^+(r) = \sum_n \begin{pmatrix} W_{n,j}^l \\ W_{N+n,j}^l \end{pmatrix} R_{nl}(r)$, and $P_l(\cos \theta_{12}) = \frac{4\pi}{2L+1} \sum_{M=-L}^L Y_{LM}^*(\theta_1, \varphi_1) Y_{LM}(\theta_2, \varphi_2)$ are the Legendre polynomials and θ_{12} is the angle between the vectors \mathbf{r}_1 and \mathbf{r}_2 . Here \hat{G} is the Green's function in the matrix form $\hat{G} = \begin{pmatrix} G_{\uparrow\uparrow} & G_{\uparrow\downarrow} \\ G_{\downarrow\uparrow} & G_{\downarrow\downarrow} \end{pmatrix}$.

The kernel $\mathcal{L}_{iklj,L}(r_1, r_3, \omega)$ of Eq. (26) is (see Appendix B):

given by

$$\gamma(r) = \frac{mk_c(r)}{2\pi^2\hbar^2} \left(\frac{\kappa(r)}{2} \log \frac{1 + \kappa(r)}{1 - \kappa(r)} - 1 \right) \quad (38)$$

where $\frac{\hbar^2 k_c(r)^2}{2m} = E_c - \frac{1}{2}m\omega_T^2 r^2$, $\frac{\hbar^2 k_F(r)^2}{2m} = \mu - \frac{1}{2}m\omega_T^2 r^2$, $\kappa(r) = k_F(r)/k_c(r)$, and $E_c = \hbar\omega_T(2N_c + 1)$ is the cut-off energy. We use cut-off energy $E_c = 60 \hbar\omega_T$ (for runs with the Hartree energy we used $E_c = 100 \hbar\omega_T$), which proved to be sufficient for studying the density response of the rather weakly interacting gas, resulting in at most 1 % error in the magnitude of the pairing field. The Fermi energy is $E_F = 24 \hbar\omega_T$ for $N = 4930$. For the interaction in the density response in Eq. (26) we use the above renormalized interaction g_0 as in Ref. [20].

IV. RESULTS

In this section we present the numerical results of the density response. In Section IV A we relate the density response with the frequency of collective excitations. In Section IV B we study the density response function for weak interactions, and in Section IV C we interpret the width of a band of collective excitations as the damping rate of the modes. In the Section IV D we show how the frequencies of the excitations depend on the interaction strength and discuss the interesting effect of merging of the pair vibration and collisionless hydrodynamic excitation branches. In the Section IV E we discuss the cases of closed and open shells (i.e. cases of different numbers of atoms).

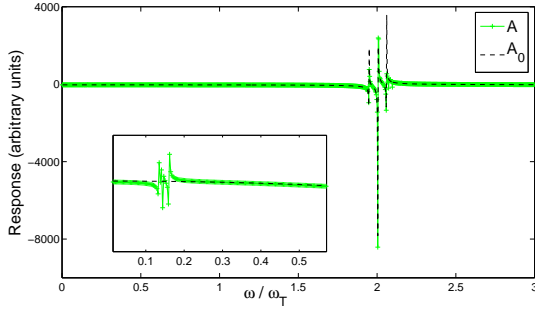


FIG. 2. (Color online) The density response in the extreme weakly interacting limit $k_F a = -0.22$ ($\Delta(0) = 0.06 \hbar \omega_T$) shows two groups of excitations. One, a prominent one, at frequencies $\omega \approx 2\omega_T$ and another (shown enlarged in the inset) at $\omega \approx 0.15\omega_T$. Shown are the full density response $\mathcal{A}(\omega)$ and the single particle response $\mathcal{A}_0(\omega)$.

A. Spectrum of the monopole mode

Our goal is to study the density response $\mathcal{A}_{ij,L}(r_1, r_5, \omega)$, which was defined in Section III B. As was discussed in Section II B, the peaks in the response function yield the frequencies of the collective excitations of the system. In order to better understand the physical origin of various excitations we will consider also the non-RPA response $\mathcal{A}_{0ij,L}(r_1, r_5, \omega)$, which was discussed in Section III B. The peaks in this function reflect the frequencies of single particle excitations. Thus in this article we will call it the single particle density response, and $\mathcal{A}_{ij,L}(r_1, r_5, \omega)$ the full density response. The simultaneous study of $\mathcal{A}_{ij,L}(r_1, r_5, \omega)$ and $\mathcal{A}_{0ij,L}(r_1, r_5, \omega)$ allows one to identify the origin of different collective excitations; some excitations in $\mathcal{A}_{ij,L}(r_1, r_5, \omega)$ have their origin in $\mathcal{A}_{0ij,L}(r_1, r_5, \omega)$ as corresponding single particle excitations, while others, which we refer to as purely collective excitations, do not have a corresponding peak in $\mathcal{A}_{0ij,L}(r_1, r_5, \omega)$.

The density response $\mathcal{A}_{ij,L}(r_1, r_5, \omega)$ depends on six parameters: spin indices i and j , the angular momentum L , positions r_1 and r_5 , and the frequency ω . In addition, the response can be calculated for three different kinds of probing fields ϕ_\uparrow , ϕ_\downarrow and η , as described in Eq. (15). However, in Section IV F we will show that the main features of the collective excitation spectra do not depend on the parameters i , j , r_1 , r_5 nor on the fields ϕ_\uparrow , ϕ_\downarrow , η , but only on the angular momentum L and the frequency ω . In this paper we will study only the monopole mode, corresponding to $L = 0$. Nevertheless, our method allows also the calculation of the response function for higher angular momenta $L > 0$. Hence we will now limit the study to $\mathcal{A}_{\uparrow\uparrow}(r_1 = 0, r_5 = 0, \omega)|_{\phi_\uparrow, L=0}$, denoting it as $\mathcal{A}(\omega)$.

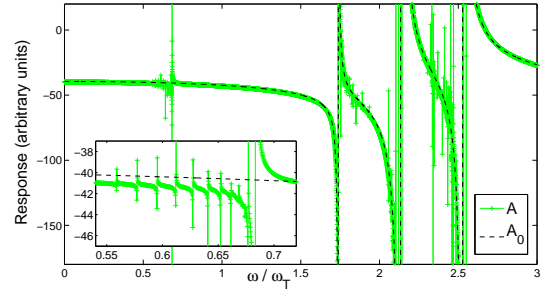


FIG. 3. (Color online) The density response for a slightly stronger interaction than in Fig. 2 $k_F a = -0.50$ ($\Delta(0) = 0.78 \hbar \omega_T$), shows the increase in the widths of the collective excitation bands (in $\mathcal{A}(\omega)$) and the separation of the single particle excitations (in $\mathcal{A}_0(\omega)$).

B. Results for weak interactions

In this chapter we study the full density response $\mathcal{A}_{\uparrow\uparrow}(\omega) = \frac{\delta \rho_\uparrow}{\delta \phi_\uparrow}$ and the corresponding single particle density response $\mathcal{A}_{0,\uparrow\uparrow}(\omega)$, which we denote as $\mathcal{A}(\omega)$ and $\mathcal{A}_0(\omega)$, respectively. From here on until further notice we consider the response for the total number of atoms $N = 4930$.

Typical results for the density response in the weakly interacting regime are shown in Figs. 2 and 3. Fig. 2 shows the full density response $\mathcal{A}(\omega)$ and the corresponding single particle density response $\mathcal{A}_0(\omega)$ for $k_F a = -0.22$. This case corresponds to the gap in the centre of the trap $\Delta(0) = 0.06 \hbar \omega_T$. In Fig. 3 are shown responses for a higher interaction $k_F a = -0.50$ (the gap in the centre of the trap $\Delta(0) = 0.78 \hbar \omega_T$).

Both figures show two groups of peaks, one at low frequencies $\omega < 2\omega_T$ and another close to $2\omega_T$. This is a typical result for sufficiently weak interactions, with the key criterion being the value of the gap $\Delta(0) < 2\hbar\omega_T$. The group of peaks in the vicinity of $2\omega_T$ is present both in the full response $\mathcal{A}(\omega)$ as well as in the single particle response $\mathcal{A}_0(\omega)$, the corresponding single particle excitations describing transitions of single atoms from the Fermi surface to the next higher oscillator energy level. These excitations are described by the hydrodynamic model for a collisionless gas. The other group of peaks at lower frequencies is shown in the insets of Figs. 2 and 3. These peaks are present only in the full density response $\mathcal{A}(\omega)$ but not in the single particle density response $\mathcal{A}_0(\omega)$ and thus these are purely collective excitations. These are called pair vibration modes and they describe pair amplitude modulations [19]. In the very weakly interacting limit the pair vibration mode frequency is given by the pairing gap as $\omega \approx 2\Delta(0)/\hbar$, but as already seen in Fig. 3 the relation does not hold for stronger interactions (see the positions of the $\mathcal{A}(\omega)$ peaks in Figs. 2 and 3 compared to $2\Delta(0)$).

Note that for the pair vibration modes we do not ob-

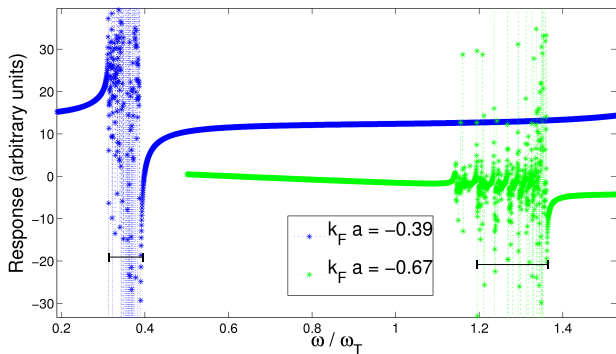


FIG. 4. (Color online) The pair vibration modes, corresponding to purely collective excitations, for $k_F a = -0.39$ ($\Delta(0) = 0.30 \hbar \omega_T$) and $k_F a = -0.67$ ($\Delta(0) = 2.26 \hbar \omega_T$). Shown are also the corresponding collective mode band widths $0.06 \omega_T$ and $0.22 \omega_T$, respectively.

serve an individual peak but rather a group of peaks close to each other. With the interaction increasing, the peaks are shifted to higher frequencies and the distance between them increases. We discuss the interaction dependence more in Section IV D.

Also the group of peaks at $\omega \approx 2 \omega_T$ experiences significant changes when the interaction is increased. Fig. 3 shows how for stronger interactions the three single particle excitations are accompanied by at least 17 peaks, corresponding to collective modes, between $\omega = 2.01 \omega_T$ and $\omega = 2.78 \omega_T$.

C. Damping rate

Excitations with similar frequencies can be coupled, resulting in a damping of the modes. Even though the excitations for a finite system manifest as poles with real energies and vanishing imaginary parts, in practice a large number of collective excitations with nearby lying frequencies cannot be distinguished. The distance between the mode frequencies within the band yields the time required for resolving the various peaks, but for time scales shorter than this the resulting real time evolution appears damped. For short time scales, the characteristic damping rate is given by the width of the collective excitation band. Fig. 4 shows the pair vibration modes for stronger interactions, revealing the gradual increase in the collective excitation band width and thus the increase in the corresponding damping rate. For $k_F a = -0.39$ ($\Delta(0) = 0.3 \hbar \omega_T$) the width is roughly $0.06 \omega_T$ and for $k_F a = -0.67$ ($\Delta(0) = 2.26 \hbar \omega_T$) the width is $0.22 \omega_T$.

Fig. 5 shows the width of the lowest frequency collective excitation band (the pair vibration mode for weak interactions) as a function of interactions (both as a function of $k_F a$ and $\Delta(0)$). While for weak interactions the band is narrow, the width increases rapidly when approaching the crossover regime $k_F a \approx -0.8$, corresponding to $\Delta(0) \approx 4 \hbar \omega_T$. Close to the crossover, where the

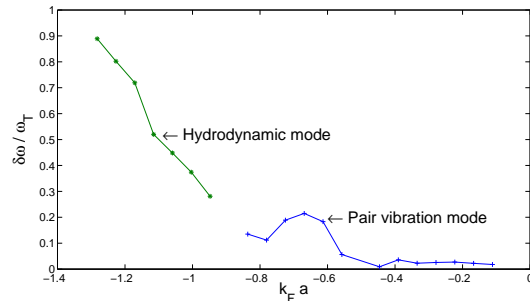


FIG. 5. (Color online) The lowest frequency collective excitation band width as a function of interactions. The band width increases rapidly when the order parameter $\Delta(0)$ approaches $4 \hbar \omega_T$ at $k_F a \approx -0.8$.

pair vibration and the hydrodynamic modes merge, the width of only the lowest excitation band may not be a good measure of the damping as the distance between the two collective mode bands is less than the widths of the two bands.

The number of peaks within the collective mode band depends on the system size, with larger systems yielding more peaks (the procedure of defining “a peak” is described in Section C). In the thermodynamic limit $N \rightarrow \infty$, we expect that the collective mode band no longer consists of separate peaks but becomes continuous. However, as long as the magnitude of the pairing gap is unchanged the width of the band is unaffected. This conjecture is supported by our calculations with higher atom numbers (up to $N = 49300$).

D. Interaction dependence

When the interaction strength increases, the two branches, the pair vibration modes and the collisionless hydrodynamic modes, approach each other and eventually merge. Instead of the Fermi energy, the relevant energy scale in this merging regime is the trap oscillator energy $\hbar \omega_T$. Subsequently the interaction strength is best measured as $\Delta(0)/\hbar \omega_T$ instead of the standard $k_F a$.

The main result of this work, Fig. 6, shows how the positions of the peaks evolve as a function of the interaction (showing both $k_F a$ and $\Delta(0)$). As discussed above, in the weakly interacting regime (here defined as the regime where $\Delta(0) < 2 \hbar \omega_T$) there are two main branches of excitations. One branch originates from the collisionless hydrodynamic excitation (or single particle excitations) at frequency $\omega = 2 \omega_T$ and the other branch describes pair vibration modes, starting from the zero frequency. For weak interactions, the latter follows the frequency $2\Delta(0)/\hbar$ [19], but the branch deviates from this asymptotic value already at $\Delta(0) \approx 0.2 \hbar \omega_T$. The collisionless hydrodynamic and the pair vibration branches merge at around $k_F a \approx -0.8$, corresponding to $\Delta(0) \approx 4 \hbar \omega_T$. For interactions beyond that, the hydrodynamic and the pair

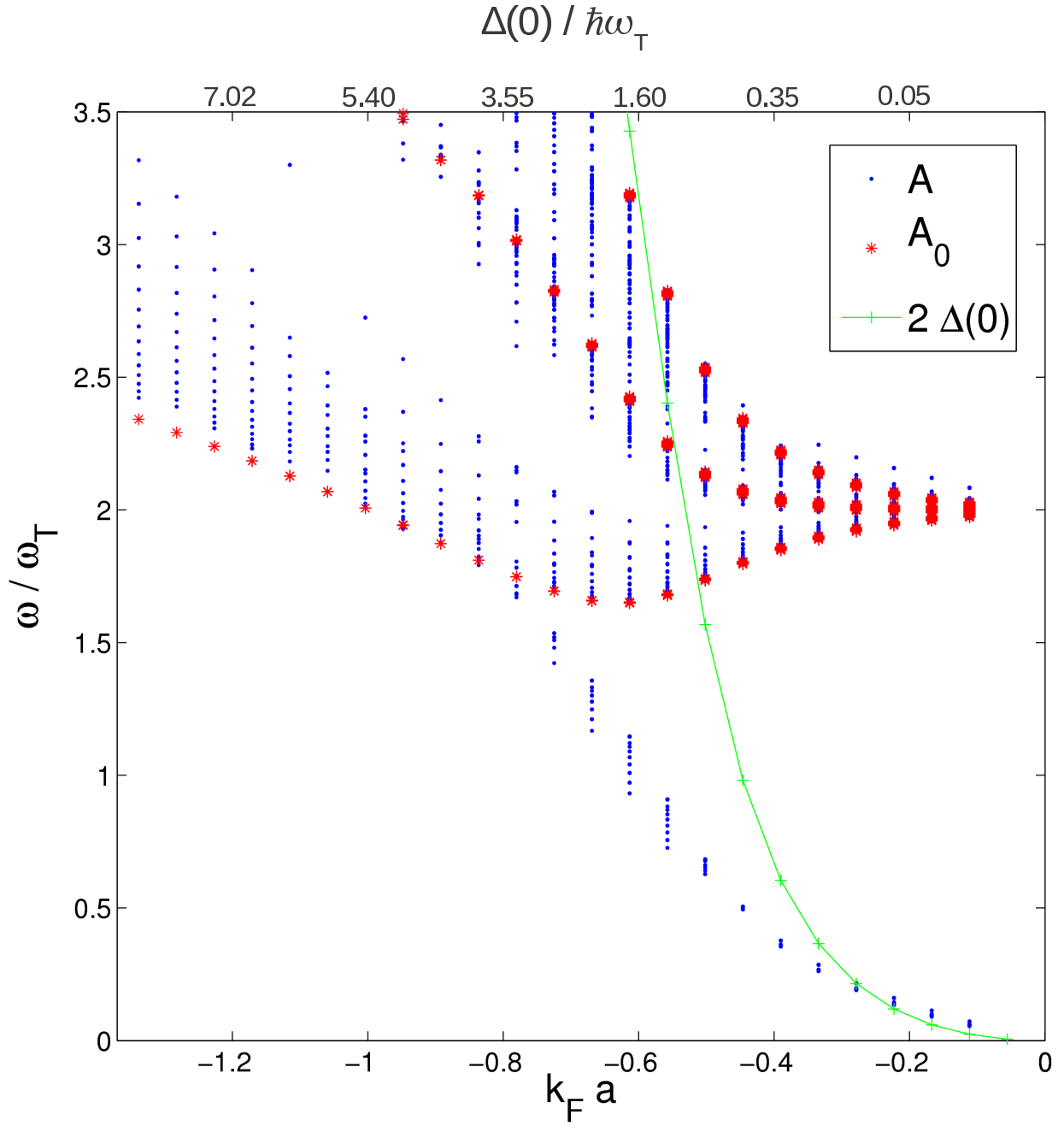


FIG. 6. (Color online) The peaks in the density responses as a function of the interaction $k_F a$ or $\Delta(0)$. The crossover from the pair vibration mode to the strongly interacting hydrodynamic mode occurs for $\Delta(0) \approx 4 \hbar \omega_T$ when the low frequency pair vibration mode merges with the weakly interacting collisionless hydrodynamic mode.

vibration modes cannot be distinguished anymore and the two modes transform into the strongly interacting Goldstone mode in the strongly interacting limit.

The crossover between the pair vibration mode and the Goldstone mode takes place when the order parameter $\Delta(0)$ is of the order of a few trap oscillator energies $\hbar \omega_T$. Since the key energy scale is given by the trap frequency instead of the Fermi energy, the crossover is realized at different interaction strengths $k_F a$ if ω_T is different. This was discussed already in Refs. [19, 20]. The

interaction strength studied in Ref. [19] corresponded to $\Delta(0) < 2 \hbar \omega_T$, whereas in Ref. [20] the monopole mode was studied for $\Delta(0) \approx 6 \hbar \omega_T$. Here we consider the crossover region between these two limits.

Notice the depression of the collective mode frequencies in the crossover regime in Fig. 6 and the increase of the collective mode band widths in Fig. 5. These effects, the suppression of the collective mode frequency and the increase in the damping rate in the crossover regime where $\Delta(0) \sim \hbar \omega_T$, are in qualitative agreement

with similar effects observed in experiments [10–12] although the symmetries of both the trap and the perturbations are different in the experimental setups. The experiment in Ref. [10] observed a dramatic increase in the damping rate and a decrease in the radial compression mode frequency at a magnetic field $B \sim 910$ G corresponding to the value $k_F a \approx -0.5$. The radial breathing mode was studied in Ref. [11], revealing a strong damping rate maximum and a depression in the collective mode frequency at a magnetic field $B \sim 1080$ G, corresponding to $k_F a \approx -0.74$. Finally, the radial quadrupole mode was studied in Ref. [12], exhibiting a damping rate maximum and a depression and a jump of the collective mode frequency at a magnetic field $B \approx 950$ G, corresponding to $k_F a \approx -0.8$. Despite the differences between the experiments in the critical interaction strengths for observing the damping rate maxima, all three experiments are in the regime where the predicted BCS pairing gap $\Delta(0)/\hbar$ is of the order of a few oscillator frequencies. However, a detailed comparison with the experiments would require a theoretical study of the same radial modes, not accessible in the present model assuming the spherical symmetry.

Fig. 7 shows the effect of the Hartree energy on the density response. The lowest energy collective mode band is shifted to higher frequencies and it is wider. This results in the crossover between the two collective mode branches occurring at a weaker interaction than when the Hartree energy was neglected. However, the qualitative features are unchanged from Fig. 6.

E. Open and closed shells

Depending on the number of the atoms, the single particle density response \mathcal{A}_0 can show significantly different behaviour. In this section we discuss the cases of closed and open shells [19]. The closed shell, which was the case discussed above with $N = 4930$, corresponds to a case in which the uppermost occupied energy level at the Fermi surface is fully occupied in the ideal noninteracting system. In contrast, in an open shell configuration (for example $N = 5600$ used below) only part of the energy level at the Fermi surface is occupied.

The two cases give very different single particle density response functions \mathcal{A}_0 in the weakly interacting limit ($\Delta(0) < 2\hbar\omega_T$). In the case of the closed shell, the lowest frequency single particle transition is the transition from the Fermi surface to the next higher n -level, corresponding to the frequency $2\omega_T$. This results in a branch of single particle excitations starting at frequency $2\omega_T$ in Fig. 6. In the case of the open shell, the energy level at the Fermi surface is also available for transitions, and the lowest energy single particle transition is a pair breaking transition in which the n quantum number is not affected. The associated energy change is proportional to $2\Delta(0)$ in the weakly interacting limit, tending to zero for vanishing interaction strength. The evolution of the peak positions

as a function of interactions for the open shell configuration is shown in the Fig. 8, revealing one single particle excitation branch starting from zero frequency and two single particle branches from the frequency $2\omega_T$. While the difference between the two shell configurations is a mesoscopic effect, the effect on the single particle excitation spectrum is artificial as the experimentally observable quantity is not \mathcal{A}_0 but the full response \mathcal{A} . Indeed, comparing the full density responses of the two configurations does not show any apparent difference, albeit the data for the open shell configuration is somewhat more noisy due to numerical issues.

F. Other response functions

In a trapped and nonuniform system the density response depends on the positions at which the perturbation is applied on and where the response is measured at. In this work we have considered the response at the centre of the trap, i.e. we defined

$$\mathcal{A}(\omega) = \mathcal{A}_{\uparrow\uparrow}(r_1 = 0, r_5 = 0, \omega)|_{\phi_{\uparrow}, L=0}. \quad (39)$$

The reason for this choice is the simplicity and the numerical efficiency, allowing the calculation of plots such as Fig. 6. In contrast, the standard measure of the density response is the strength function, which is obtained by integrating the density response over the whole trap

$$\mathcal{A}^S(\omega) = \int d\mathbf{r}_1 d\mathbf{r}_5 \mathcal{A}_{\uparrow\uparrow}(r_1, r_5, \omega)|_{\phi_{\uparrow}, L=0}. \quad (40)$$

The two definitions, Eqs. (39) and (40) produce slightly different results, but the main features of the full density response are the same: the frequencies and the widths of the collective mode bands are the same for both as shown in Fig. 9. The reason for the similarities between two methods is that the generalized random phase approximation couples the excitations at the centre of the trap to excitations all over the system, and hence one can excite for example surface modes even by considering only the centre of the trap. Such indirect effects come at the cost of reducing the amplitude of the corresponding collective mode peaks. However, when considering only the frequencies and the widths of the collective excitation bands, the actual amplitudes of various peaks are irrelevant.

In contrast, looking only at single particle excitations \mathcal{A}_0 , the local response (at the centre of the trap) has only three low energy branches, whereas the 'single-particle' strength function $\mathcal{A}_0^S = \int d\mathbf{r}_1 d\mathbf{r}_5 \mathcal{A}_0(r_1, r_5, \omega)$ has a large number of peaks, corresponding to single-particle excitations at different parts of the trap. Without the coupling provided by the generalized random phase approximation, the single-particle excitations localized at the centre of the trap will remain localized. The single particle excitation spectra are thus clearly different in the two approaches. However, the experimentally relevant quantity is the full density response.

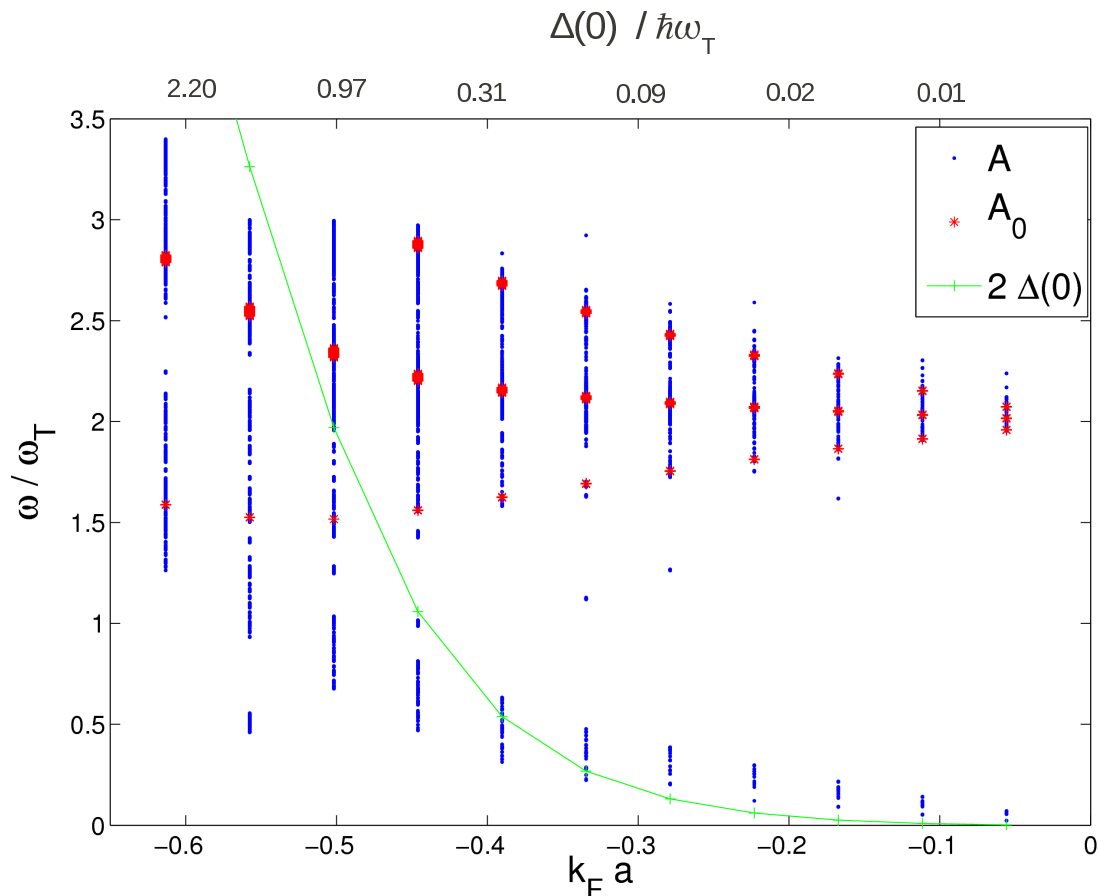


FIG. 7. (Color online) The peaks in the density responses as a function of the interaction $k_F a$ or $\Delta(0)$, including the Hartree energy contribution. The Hartree energy compresses the gas, resulting in a larger order parameter $\Delta(0)$. Comparing with Fig. 6, this shifts the crossover from the pair vibration mode to the strongly interacting hydrodynamic mode to lower interaction strengths.

The density response results discussed in this manuscript have considered only the response to probing field ϕ_\uparrow directly affecting only the density of spin- \uparrow atoms. Fig. 10 shows the response for all three probing fields ϕ_\uparrow , ϕ_\downarrow and η , as described in Eq. (15). While the magnitudes of the individual peaks are different for different probing fields, the main features of the responses are the same, namely the frequencies and the widths of the collective excitation bands. The same is true also when considering the response of the pairing field.

V. DISCUSSION

In this work, we have used the random phase approximation together with the self-consistent Bogoliubov-deGennes method for studying the density response of a trapped Fermi gas. Concentrating on the monopole mode in a spherically symmetric trap we have analysed in detail the interesting crossover regime in which the collisionless gas becomes strongly interacting. We observe the merging of a pair vibration mode, originating

from a low frequency excitation in the extreme weakly interacting gas, and a collisionless hydrodynamic mode at frequency $2\omega_T$, the combined collective mode eventually becoming the strongly interacting hydrodynamic Goldstone mode in the unitary regime. The merging of the two collective mode branches is signalled by a depression of the mode frequencies and an increase in the damping rate, in good agreement with the experiments done in elongated traps. In the future it will be interesting to generalise the method to non-spherically symmetric systems [26–29], allowing the study of various radial and axial modes and thus a more detailed comparison with the reported and possibly new experiments. Other interesting future extensions of the method are studies of the FFLO state [30, 31], sensor applications [32] and dimensionality effects [33].

ACKNOWLEDGEMENTS

We would like to acknowledge useful discussions with M.O.J. Heikkinen. This work was supported by Na-

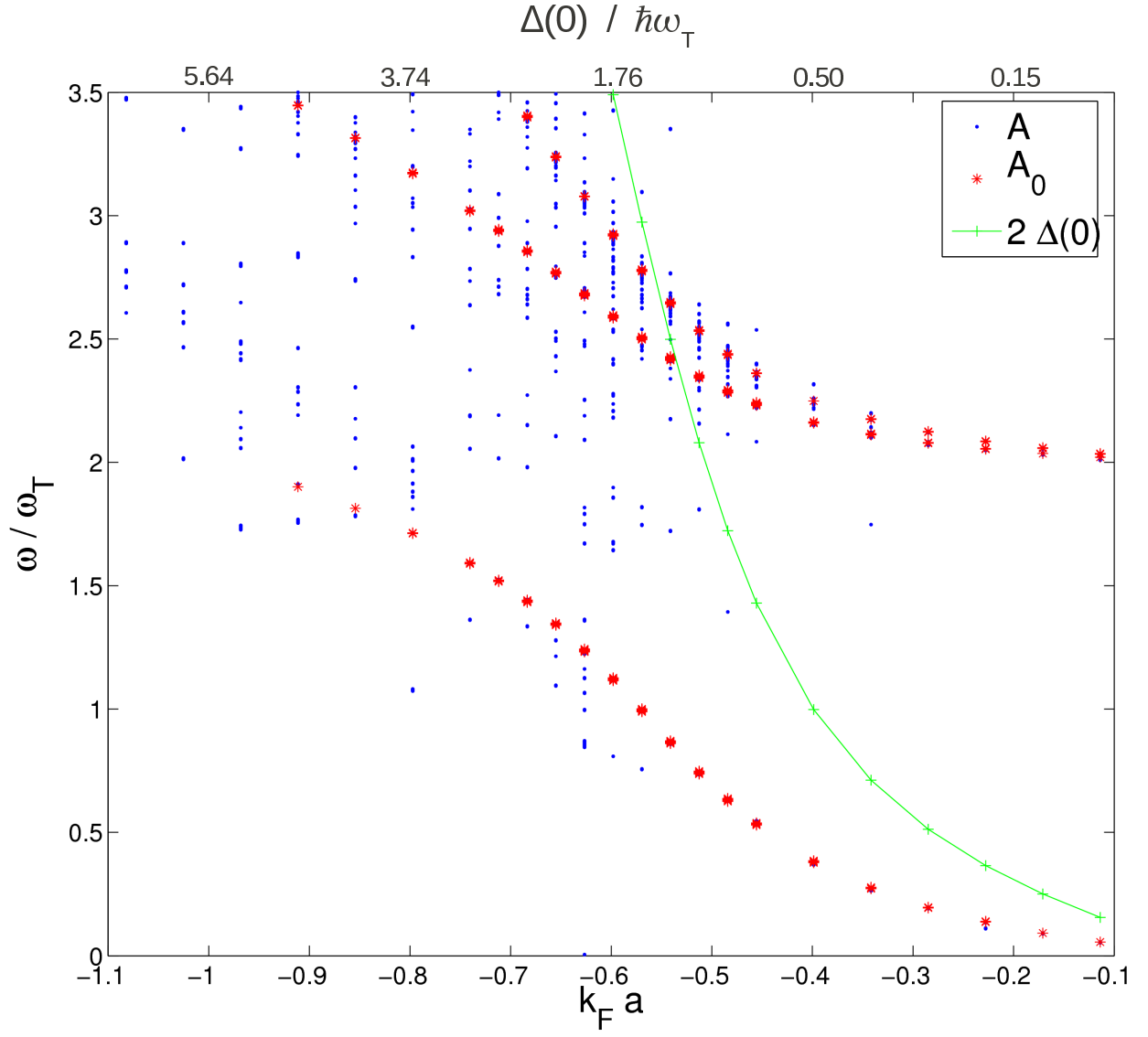


FIG. 8. (Color online) The peaks of the density response as function of interactions for open shell configuration. The full density response is similar (albeit more noisy) to the closed shell configuration in Fig. 6, but here one of the single-particle excitation branches follows the pair vibration mode frequency at weak interactions ($\Delta(0) < 4 \hbar \omega_T$).

tional Graduate School in Materials Physics and the Academy of Finland (Project Nos. 210953, 213362, 217043, 217045, 135000, and 141039), conducted as a

part of a EURI scheme grant, see www.esf.org/euryi, and supported in part by the National Science Foundation under Grant No. PHY05-51164.

-
- [1] A. Griffin, W.-C. Wu, and S. Stringari, Phys. Rev. Lett. **78**, 1838 (1997).
 - [2] M. A. Baranov and D. S. Petrov, Phys. Rev. A **62**, 041601 (2000).
 - [3] G. M. Bruun and C. W. Clark, Phys. Rev. Lett. **83**, 5415 (1999).
 - [4] S. Stringari, Europhys. Lett. **65**, 749 (2004).
 - [5] A. Bulgac and G. F. Bertsch, Phys. Rev. Lett. **94**, 070401 (2005).
 - [6] J. Kinast, S. L. Hemmer, M. E. Gehm, A. Turlapov, and J. E. Thomas, Phys. Rev. Lett. **92**, 150402 (2004).
 - [7] J. Kinast, A. Turlapov, and J. E. Thomas, Phys. Rev. Lett. **94**, 170404 (2005).
 - [8] A. Altmeyer, S. Riedl, C. Kohstall, M. J. Wright, R. Geursen, M. Bartenstein, C. Chin, J. H. Denschlag, and R. Grimm, Phys. Rev. Lett. **98**, 040401 (2007).
 - [9] M. J. Wright, S. Riedl, A. Altmeyer, C. Kohstall, E. R. S. Guajardo, J. H. Denschlag, and R. Grimm, Phys. Rev. Lett. **99**, 150403 (2007).

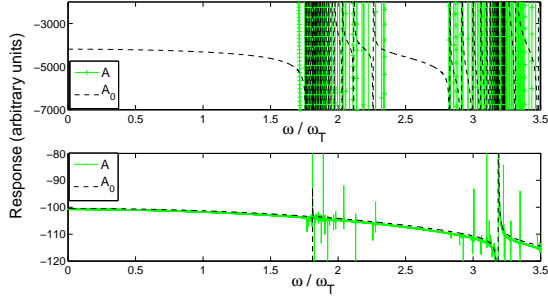


FIG. 9. (Color online) The density response determined using the strength function in Eq. (40) (upper figure) produces the same qualitative features as the definition used in this work in which the response is considered only at the centre of the trap (lower figure). Here $k_F a = -0.84$ and $\Delta(0) = 3.9 \hbar \omega_T$.

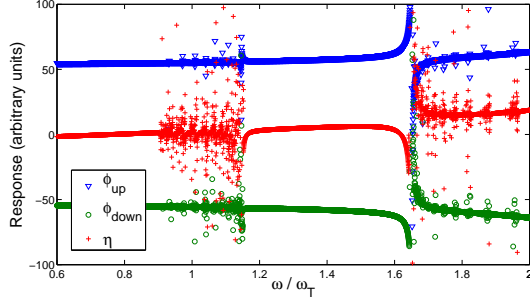


FIG. 10. (Color online) The density responses $\mathcal{A}(\omega)$ for different probing fields ϕ_\uparrow , ϕ_\downarrow and η for $k_F a = -0.61$ produce the same collective excitation bands.

- [10] M. Bartenstein, A. Altmeyer, S. Riedl, S. Jochim, C. Chin, J. H. Denschlag, and R. Grimm, Phys. Rev. Lett. **92**, 203201 (2004).
 [11] J. Kinast, A. Turlapov, and J. E. Thomas, Phys. Rev. A **70**, 051401 (2004).
 [12] A. Altmeyer, S. Riedl, M. J. Wright, C. Kohstall, J. H. Denschlag, and R. Grimm, Phys. Rev. A **76**, 033610 (2007).
 [13] R. Combescot and X. Leyronas, Phys. Rev. Lett. **93**, 138901 (2004).

- [14] P. W. Anderson, Phys. Rev. **112**, 1900 (1958).
 [15] A. Minguzzi, G. Ferrari, and Y. Castin, Eur. Phys. J. D **17**, 49 (2001).
 [16] G. M. Bruun and B. R. Mottelson, Phys. Rev. Lett. **87**, 270403 (2001).
 [17] M. Rodriguez and P. Törmä, Phys. Rev. A **66**, 033601 (2002).
 [18] G. M. Bruun and H. Smith, Phys. Rev. A **76**, 045602 (2007).
 [19] G. M. Bruun, Phys. Rev. Lett. **89**, 263002 (2002).
 [20] M. Grasso, E. Khan, and M. Urban, Phys. Rev. A **72**, 043617 (2005).
 [21] F. Serwane, G. Zürn, T. Lompe, T. B. Ottenstein, A. N. Wenz, and S. Jochim, Science **332**, 336 (2011).
 [22] R. Côté and A. Griffin, Phys. Rev. B **48**, 10404 (1993).
 [23] S. Giorgini, L. P. Pitaevskii, and S. Stringari, Rev. Mod. Phys. **80**, 1215 (2008).
 [24] L. M. Jensen, J. Kinnunen, and P. Törmä, Phys. Rev. A **76**, 033620 (2007).
 [25] M. Grasso and M. Urban, Phys. Rev. A **68**, 033610 (2003).
 [26] M. Tezuka, Y. Yanase, and M. Ueda, arXiv:0811.1650v3(2010).
 [27] L. O. Baksmaty, H. Lu, C. J. Bolech, and H. Pu, Phys. Rev. A **83**, 023604 (2011).
 [28] D.-H. Kim, J. J. Kinnunen, J.-P. Martikainen, and P. Törmä, Phys. Rev. Lett. **106**, 095301 (2011).
 [29] L. O. Baksmaty, H. Lu, C. J. Bolech, and H. Pu, New J. Phys. **13**, 055014 (2011).
 [30] J. M. Edge and N. R. Cooper, Phys. Rev. Lett. **103**, 065301 (2009).
 [31] M. O. J. Heikkinen and P. Törmä, Phys. Rev. A **83**, 053630 (2011).
 [32] T. K. Koponen, J. Pasanen, and P. Törmä, Phys. Rev. Lett. **102**, 165301 (2009).
 [33] T. Koponen, J.-P. Martikainen, J. Kinnunen, and P. Törmä, Phys. Rev. A **73**, 033620 (2006).

Appendix A: Density response within the Random Phase Approximation

In this appendix we discuss the derivation of the density response Eq. (23), starting from the Hamiltonian in Eq. (11). The Green's function $\hat{G}(\mathbf{1}, \mathbf{2})$ satisfies the following equation

$$\left(-\frac{\partial}{\partial \tau_1} + \left(\frac{\nabla_1^2}{2m} + \mu - \frac{m\omega_T^2 x_1^2}{2} \right) \tau_3 \right) \hat{G}(\mathbf{1}, \mathbf{2}) = \hat{I} \delta(\mathbf{1} - \mathbf{2}) + \hat{W}(\mathbf{1}) \hat{G}(\mathbf{1}, \mathbf{2}) + g_0 \hat{M}_{\text{int}}(\mathbf{1}, \mathbf{2}), \quad (\text{A1})$$

where \hat{I} is the identity operator,

$$\hat{W}(\mathbf{1}) = \begin{pmatrix} -e\phi_\uparrow(\mathbf{1}) & \eta^*(\mathbf{1}) \\ \eta(\mathbf{1}) & e\phi_\downarrow(\mathbf{1}) \end{pmatrix}, \quad (\text{A2})$$

and

$$\begin{aligned} \hat{M}_{\text{int}}(\mathbf{1}, \mathbf{2}) &= \\ &= \begin{pmatrix} \langle T\psi_\uparrow^\dagger(\mathbf{2})n(\mathbf{1})\psi_\uparrow(\mathbf{1}) \rangle & \langle T\psi_\downarrow(\mathbf{2})n(\mathbf{1})\psi_\uparrow(\mathbf{1}) \rangle \\ -\langle T\psi_\uparrow^\dagger(\mathbf{2})\psi_\downarrow^\dagger(\mathbf{1})n(\mathbf{1}) \rangle & \langle T\psi_\downarrow^\dagger(\mathbf{1})n(\mathbf{1})\psi_\downarrow(\mathbf{2}) \rangle \end{pmatrix}, \end{aligned} \quad (\text{A3})$$

where $\langle T \dots \rangle$ is a time-ordered correlator. The bare Green's function $\hat{G}_0(\mathbf{1}, \mathbf{2})$ is defined similarly but in the absence of the perturbation and the interactions $g_0 = 0$

$$\left(-\frac{\partial}{\partial \tau_1} + \left(\frac{\nabla_1^2}{2m} + \mu - \frac{m\omega_T^2 x_1^2}{2} \right) \tau_3 \right) \hat{G}_0(\mathbf{1}, \mathbf{2}) = \hat{I} \delta(\mathbf{1} - \mathbf{2}). \quad (\text{A4})$$

Now, we can express Eq. (A1) using $\hat{G}_0(\mathbf{1}, \mathbf{2})$ as follows

$$\begin{aligned} \hat{G}(\mathbf{1}, \mathbf{2}) &= \hat{G}_0(\mathbf{1}, \mathbf{2}) \\ &+ \int d\mathbf{3} \int d\mathbf{4} \hat{G}_0(\mathbf{1}, \mathbf{3}) \hat{W}(\mathbf{3}) \delta(\mathbf{3} - \mathbf{4}) \hat{G}(\mathbf{4}, \mathbf{2}) \\ &+ g_0 \int d\mathbf{3} \int d\mathbf{4} \hat{G}_0(\mathbf{1}, \mathbf{3}) \hat{\Sigma}(\mathbf{3}, \mathbf{4}) \hat{G}(\mathbf{4}, \mathbf{2}), \end{aligned} \quad (\text{A5})$$

where the self-energy $\hat{\Sigma}(\mathbf{3}, \mathbf{4}) = \int d\mathbf{5} \hat{M}_{\text{int}}(\mathbf{3}, \mathbf{5}) \hat{G}^{-1}(\mathbf{5}, \mathbf{4})$. Eq. (A5) can be formally written as

$$\hat{G}^{-1}(\mathbf{1}, \mathbf{2}) = \hat{G}_0^{-1}(\mathbf{1}, \mathbf{2}) - \hat{W}(\mathbf{1}) \delta(\mathbf{1} - \mathbf{2}) - \hat{\Sigma}(\mathbf{1}, \mathbf{2}). \quad (\text{A6})$$

The next step is to apply the variational derivative $\frac{\delta}{\delta h(\mathbf{5})}$ to both sides of Eq. (A6) for separate cases $h = \phi_\uparrow; \phi_\downarrow; \eta$. Applying $\frac{\delta \hat{G}(\mathbf{1}, \mathbf{2})}{\delta h(\mathbf{5})} = - \int d\mathbf{3} d\mathbf{4} \hat{G}(\mathbf{1}, \mathbf{3}) \frac{\delta \hat{G}^{-1}(\mathbf{3}, \mathbf{4})}{\delta h(\mathbf{5})} \hat{G}(\mathbf{4}, \mathbf{2})$ yields the equation

$$\begin{aligned} \frac{\delta \hat{G}(\mathbf{1}, \mathbf{2})}{\delta h(\mathbf{5})} &= \hat{A}_0(\mathbf{1}, \mathbf{2}, \mathbf{5}) \\ &+ \int d\mathbf{3} \hat{G}(\mathbf{1}, \mathbf{3}) \left(-\tau_3 \left(-\frac{\delta n(\mathbf{3})}{\delta h(\mathbf{5})} + \frac{\delta \hat{G}(\mathbf{3}, \mathbf{3})}{\delta h(\mathbf{5})} \tau_3 \right) \right) \hat{G}(\mathbf{3}, \mathbf{2}). \end{aligned} \quad (\text{A7})$$

Here $\hat{A}_0(\mathbf{1}, \mathbf{2}, \mathbf{5})$ depends from the field h , and is $\hat{G}(\mathbf{1}, \mathbf{5}) \begin{pmatrix} 1 & 0 \\ 0 & 0 \end{pmatrix} \hat{G}(\mathbf{5}, \mathbf{2})$, $\hat{G}(\mathbf{1}, \mathbf{5}) \begin{pmatrix} 0 & 0 \\ 0 & 1 \end{pmatrix} \hat{G}(\mathbf{5}, \mathbf{2})$,

$\hat{G}(\mathbf{1}, \mathbf{5}) \begin{pmatrix} 0 & 1 \\ 1 & 0 \end{pmatrix} \hat{G}(\mathbf{5}, \mathbf{2})$ for h equal to ϕ_\uparrow , ϕ_\downarrow and η , respectively.

After transforming $\tilde{G}(\mathbf{1}, \mathbf{3}) = \tau_3 \hat{G}(\mathbf{1}, \mathbf{3})$, Eq. (A7) becomes:

$$\begin{aligned} \tilde{A}_{ij}(\mathbf{1}, \mathbf{2}, \mathbf{5}) &= \tilde{A}_{0ij}(\mathbf{1}, \mathbf{2}, \mathbf{5}) \\ &+ g_0 \int d\mathbf{3} L_{ikkj}(\mathbf{1}, \mathbf{2}, \mathbf{3}) \tilde{A}_{ll}(\mathbf{3}, \mathbf{3}, \mathbf{5}) \\ &- g_0 \int d\mathbf{3} L_{iklj}(\mathbf{1}, \mathbf{2}, \mathbf{3}) \tilde{A}_{kl}(\mathbf{3}, \mathbf{3}, \mathbf{5}), \end{aligned} \quad (\text{A8})$$

where $\tilde{A}_{ij}(\mathbf{1}, \mathbf{2}, \mathbf{5}) = \frac{\delta \tilde{G}_{ij}(\mathbf{1}, \mathbf{2})}{\delta h(\mathbf{5})}$, $L_{iklj}(\mathbf{1}, \mathbf{2}, \mathbf{3}) = \tilde{G}_{ik}(\mathbf{1}, \mathbf{3}) \tilde{G}_{lj}(\mathbf{3}, \mathbf{2})$ and $\tilde{A}_0(\mathbf{1}, \mathbf{2}, \mathbf{5}) = \tilde{G}(\mathbf{1}, \mathbf{5}) \begin{pmatrix} 1 & 0 \\ 0 & 0 \end{pmatrix} \tilde{G}(\mathbf{5}, \mathbf{2})$, $\tilde{G}(\mathbf{1}, \mathbf{5}) \begin{pmatrix} 0 & 0 \\ 0 & 1 \end{pmatrix} \tilde{G}(\mathbf{5}, \mathbf{2})$, $\tilde{G}(\mathbf{1}, \mathbf{5}) \begin{pmatrix} 0 & 1 \\ 1 & 0 \end{pmatrix} \tilde{G}(\mathbf{5}, \mathbf{2})$ for $h = \phi_\uparrow$, ϕ_\downarrow and η , respectively.

Appendix B: Coefficients $\mathcal{L}_{iklj, L}(r_1, r_3, \omega)$ via BdG Green's functions

The Fourier transform of the matrix element L_{iklj} is $L_{iklj}(\mathbf{r}_1, \mathbf{r}_3, \omega) = \frac{1}{\beta \hbar} \sum_{\Omega_n} G_{ik}(\mathbf{r}_1, \mathbf{r}_3, \Omega_n) G_{lj}(\mathbf{r}_3, \mathbf{r}_1, \omega + \Omega_n)$, where $\beta = \frac{1}{k_B T}$ is the temperature, and $\Omega_n = \frac{(2n+1)\pi}{\beta \hbar}$ are Matsubara frequencies. As discussed in Section IIIB, the spherical symmetry allows a great simplification of the problem, and one needs only to solve the coefficients $\mathcal{L}_{iklj, L}(r_1, r_3, \omega) = \int d\gamma_{13} \sin \gamma_{13} L_{iklj}(\mathbf{r}_1, \mathbf{r}_3, \omega) P_L(\cos \gamma_{13})$, which can be written as

$$\begin{aligned} \mathcal{L}_{iklj, L}(r_1, r_3, \omega) &= (2L+1) \frac{1}{\beta \hbar} \sum_{L_1 L_2} \begin{pmatrix} L & L_1 & L_2 \\ 0 & 0 & 0 \end{pmatrix}^2 \times \\ &\sum_{\Omega_n} G_{ik, L_1}(r_1, r_3, \Omega_n) G_{lj, L_2}(r_3, r_1, \omega + \Omega_n), \end{aligned} \quad (\text{B1})$$

where $\begin{pmatrix} L & L_1 & L_2 \\ 0 & 0 & 0 \end{pmatrix}$ are Wigner 3j coefficients.

The Bogoliubov-deGennes Green's functions are provided by Eq. (36), yielding the final result

$$\begin{aligned} \mathcal{L}_{iklj, L}(r_1, r_3, \omega) &= (2L+1) \sum_{L_1 L_2} \begin{pmatrix} L & L_1 & L_2 \\ 0 & 0 & 0 \end{pmatrix}^2 \frac{2L_1+1}{4\pi} \frac{2L_2+1}{4\pi} \\ &\times \sum_{J_1 J_2} \left(\lambda_{J_1 L_1, ik}^- \lambda_{J_2 L_2, lj}^- \frac{n_F(E_{J_1 L_1}) - n_F(E_{J_2 L_2})}{\omega + E_{J_1 L_1} - E_{J_2 L_2}} + \lambda_{J_1 L_1, ik}^+ \lambda_{J_2 L_2, lj}^+ \frac{n_F(-E_{J_1 L_1}) - n_F(-E_{J_2 L_2})}{\omega - E_{J_1 L_1} + E_{J_2 L_2}} \right. \\ &\left. + \lambda_{J_1 L_1, ik}^- \lambda_{J_2 L_2, lj}^+ \frac{n_F(E_{J_1 L_1}) - n_F(-E_{J_2 L_2})}{\omega + E_{J_1 L_1} + E_{J_2 L_2}} + \lambda_{J_1 L_1, ik}^+ \lambda_{J_2 L_2, lj}^- \frac{n_F(-E_{J_1 L_1}) - n_F(E_{J_2 L_2})}{\omega - E_{J_1 L_1} - E_{J_2 L_2}} \right), \end{aligned} \quad (\text{B2})$$

where $\lambda_{J_1 L_1, ik}^\pm = \Lambda_{J_1 L_1, i}^\pm(r_1) \Lambda_{J_1 L_1, k}^{\pm\dagger}(r_3)$, $\lambda_{J_2 L_2, lj}^\pm = \Lambda_{J_2 L_2, l}^\pm(r_3) \Lambda_{J_2 L_2, j}^{\pm\dagger}(r_1)$, and the quasiparticle wavefunc-

tions Λ^\pm are defined in the main text below Eq. (36).

Appendix C: Procedure of defining the peaks

Numerical calculations with very high precision show that the peaks in the density response have the shape $\sim \frac{1}{(\omega - \omega_0)^n}$ where ω_0 is the (yet unknown) frequency of the mode. However, for most of the figures in this work, we have limited the frequency grid resolution to $\delta\omega = 3 \cdot 10^{-4} \omega_T$. This resolution is high enough to show the existence of a peak but not to show the detailed shape. For this resolution, some modes result in extremely high peaks (if the frequency grid happened to coincide with the mode frequency) regardless of the ac-

tual prefactor or the amplitude. We decided to define 'a peak' as a frequency for which the derivative of the density response is higher than some chosen cut-off. The reason for using the derivative instead of the height of the peak is that the base level of the response (the value of the response in areas away from any peaks) is slowly changing with increasing frequency ω . Such slow changes in the base level do not affect the derivative and the peaks are more clearly seen. The caveat is the higher sensitivity to numerical noise. For creating Figs. 6 and 8 we mark a peak when the derivative $\frac{\partial A(\omega)}{\partial \omega} > 3 \cdot 10^3$. The choice of this value is a compromise between limiting the required resolution and in avoiding the effect of the numerical noise. The main results, such as the frequencies of the collective modes or the widths of the excitation bands, are not sensitive to this choice.